

Investigation of the Electronic and Vibrational Structures of the 2-Furanyloxy Radical Using Photoelectron Imaging and Photodetachment Spectroscopy via the Dipole-Bound State of the 2-Furanyloxide Anion

Yue-Rou Zhang, Dao-Fu Yuan,* and Lai-Sheng Wang*



Cite This: *J. Phys. Chem. Lett.* 2022, 13, 11481–11488



Read Online

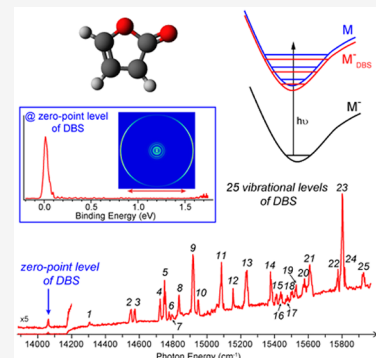
ACCESS |

Metrics & More

Article Recommendations

Supporting Information

ABSTRACT: The 2-furanyloxy radical is an important chemical reaction intermediate in the combustion of biofuels and aromatic compounds. We report an investigation of its electronic and vibrational structures using photoelectron and photodetachment spectroscopy and resonant photoelectron imaging (PEI) of cryogenically cooled 2-furanyloxide anion. The electron affinity of 2-furanyloxy is measured to be 1.7573(8) eV. Two excited electronic states are observed at excitation energies of 2.14 and 2.82 eV above the ground state. Photodetachment spectroscopy reveals a dipole-bound state 0.0143 eV below the detachment threshold and 25 vibrational Feshbach resonances for the 2-furanyloxide anion. The combination of photodetachment spectroscopy and resonant PEI yields frequencies for 18 out of a total of 21 vibrational modes for the 2-furanyloxy radical, including all six of its bending modes. The rich electronic and vibrational information will be valuable for further understanding the role of 2-furanyloxy as a key reaction intermediate of combustion and atmospheric interests.



With the unsustainable environmental cost of fossil fuel consumption, there is an urgent need to develop renewable energy sources to meet the increasing energy demand of the world. Biomass is an attractive renewable energy source.^{1–3} In particular, furan derivatives (including alkylated furans and furanic ethers) derived from nonedible biomass are important platform chemicals for biofuels.^{4–7} Understanding and characterizing the intermediates in the biomass conversion processes and combustion of biofuels are challenging but critical for the development of biomass as an alternative energy source. The 2-furanyloxy radical ($\text{C}_4\text{H}_3\text{O}_2^\bullet$, Figure S1) is an important combustion intermediate of biofuels involving furan and its derivatives or aromatic compounds.^{8–13} The 2-furanyloxy radical can be readily produced by pyrolysis of 2-methoxyfuran due to the weak O–CH₃ bond.^{14–16} The 2-furanyloxy radical is stabilized due to the delocalization of the unpaired electron over the carbon atoms on the furanic ring^{9–11,17} and it can be viewed as an allylic lactone (Figure S1b), rather than an alkoxy radical. Ellison and co-workers first observed the 2-furanyloxy radical experimentally from pyrolysis of 2-methoxyfuran using VUV photoionization mass spectrometry.¹⁸ They also studied its pyrolysis pathways and characterized it using matrix isolation infrared spectroscopy and photoionization efficiency studies, obtaining several vibrational frequencies in an Ar matrix and its ionization energy. Subsequently, Zwier and co-workers characterized the 2-furanyloxy radical using broadband microwave spectroscopy in a supersonic beam with a flash pyrolysis source.¹⁹ They

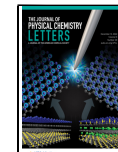
obtained its rotational constants and confirmed that the 2-furanyloxy radical can indeed be considered as an allylic lactone, where the unpaired spin is mainly delocalized on the carbons of the furanic ring rather than the O atom of the methoxy group. However, there are no other experimental studies on this important radical intermediate. Its electronic and spectroscopic properties, which are critical to understanding its reactivity, still remain poorly understood.

High-resolution photoelectron spectroscopy (PES) of cold closed-shell anions is a powerful experimental technique to probe the electronic and vibrational spectroscopy of radical species.²⁰ In particular, the combination of PES, photodetachment spectroscopy (PDS), and resonant-PES (rPES) via dipole-bound states (DBSs) of polar anions has proven to be an even more powerful technique to obtain vibronic information for polar radical species.²¹ Polar molecules with dipole moments larger than 2.5 D can weakly bind an electron in a diffuse orbital.^{22–26} Valence-bound anions can possess DBSs as electronically excited states near the detachment threshold,²⁷ analogous to the Rydberg state in a neutral

Received: November 8, 2022

Accepted: December 2, 2022

Published: December 5, 2022



molecule. Such excited DBSs were first observed in PDS of organic anions and allowed high-resolution PDS via rotational autodetachment.^{28–32} vibrationally cold anions made possible by cryogenic cooling have allowed vibrational autodetachment spectroscopy,³³ in particular, rPES via above-threshold vibrational levels of the DBS,²¹ which can result in much richer spectroscopic information than conventional PES. Since the first observation of state-specific vibrational autodetachment in rPES of cryogenically cooled phenoxide,³⁴ DBSs have been investigated extensively in Wang's group by combining photoelectron imaging (PEI), PDS, and rPES, yielding spectroscopic information for a wide range of molecular and radical species.^{35–41} The 2-furanyloxy radical possesses a dipole moment of 4.13 D,¹⁹ which makes it possible for us to deploy the arsenal of PEI, PDS, and rPES to probe its electronic and vibrational spectroscopy using the DBS of its anion, 2-furanyloxide.

The experiment was conducted using our third-generation electrospray ionization PES (ESI-PES) apparatus,⁴² which couples a cryogenically cooled Paul trap and a high-resolution PEI system.^{43,44} The 2-furanyloxide anions were produced from ESI of a solution of 2-(trimethylsiloxy)furan. More experimental details are given in the Supporting Information. Figure 1 presents a set of photoelectron images and spectra of

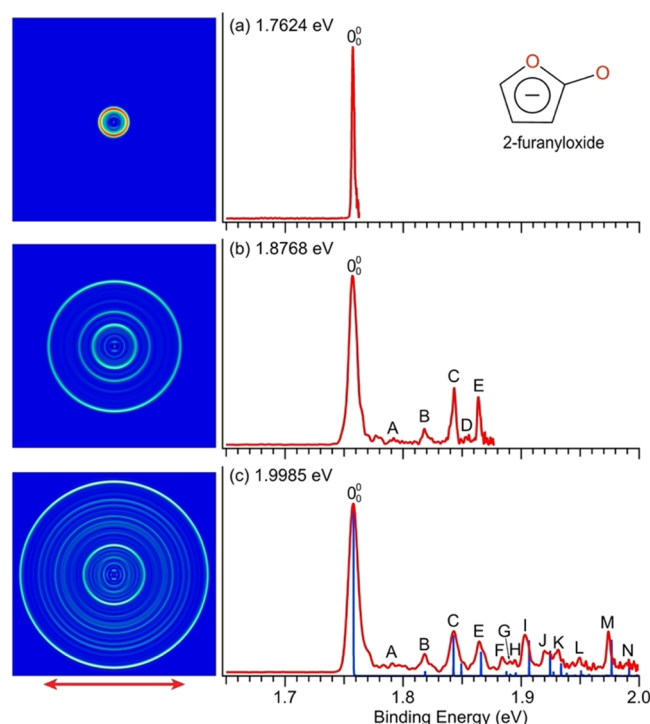


Figure 1. Photoelectron images and spectra of 2-furanyloxide at (a) $14\ 215\ \text{cm}^{-1}$ (1.7624 eV), (b) $15\ 138\ \text{cm}^{-1}$ (1.8768 eV), and (c) $16\ 119\ \text{cm}^{-1}$ (1.9985 eV). The vertical lines in (c) are the computed Franck–Condon factors. The double arrow below the images indicates the laser polarization.

cryogenically cooled 2-furanyloxide at low photon energies. The spectrum in Figure 1a taken at $14\ 215\ \text{cm}^{-1}$ (1.7624 eV) is near the detachment threshold, yielding an accurate electron affinity (EA) of $14\ 174 \pm 6\ \text{cm}^{-1}$ ($1.7573 \pm 0.0008\ \text{eV}$) for the 2-furanyloxy radical. Figure 1b,c shows two spectra at successively higher photon energies, revealing vibrational structures for the detachment transition from the ground

state of 2-furanyloxide (\tilde{X}_a) to that of the 2-furanyloxy radical (\tilde{X}). Fourteen vibrational peaks are observed up to a binding energy of 2.0 eV, labeled from A to N. The vibrational peaks A and D are negligible and are in fact only well resolved in the resonant PES data (*vide infra*).

A spectrum taken at an even higher photon energy of $21\ 119\ \text{cm}^{-1}$ (2.6185 eV), covering the full Franck–Condon (FC) region of the ground state transition, is shown in Figure S2 in comparison with an FC simulation. Additionally, the computed FC factors are also compared with the higher resolution spectrum at $16\ 119\ \text{cm}^{-1}$ in Figure 1c. The FC factors were calculated using the FC-Lab2 program⁴⁵ and the calculated geometries of the anion and neutral ground state (Figure S1) and the calculated frequencies of the neutral ground state (Table S5). The structure of 2-furanyloxy (Figure S1b) calculated at the B3LYP level in the current study is similar to that computed at a higher level of theory reported previously.¹⁹ The allylic lactone nature of the 2-furanyloxy radical (Figure S1b) is clearly shown by the calculated bond lengths. Interestingly, the 2-furanyloxide anion (Figure S1a) can also be viewed as a lactone, with the extra electron delocalized on the carbon atoms of the furanic ring. There are significant bond length changes from the anion to the neutral ground state, consisting with the relatively broad FC activity. In general, the computed FC factors agree well with the PES data, allowing the resolved vibrational peaks to be readily assigned. All the observed PES features are due to symmetry-allowed vibrational levels (a' symmetry), except for the weak peaks A and D, which are due to the out-of-plane bending modes ν_{21} (a'') and ν_{17} (a''), respectively. These modes are symmetry-forbidden, which is why peaks A and D are so weak. The four most FC-active modes are ν_{14} (peak C), ν_{12} (peak E), ν_8 (peak I), and ν_4 (peak M). The observed vibrational peaks from the PES data and their binding energies and assignments are given in Table S1. The good agreement between the calculated FC profile and the observed spectra indicates that there is no significant vibronic coupling between the \tilde{X} ground state and the excited electronic states of 2-furanyloxy, quite different from the case of triazolide reported recently.^{46,47}

Figure 2 displays the PE image and spectrum of 2-furanyloxide at 4.661 eV. In addition to the ground state transition (\tilde{X}), two excited state transitions (\tilde{A} , \tilde{B}) are also observed at higher binding energies. The weak features from 3.9 to 4.5 eV should correspond to vibronic transitions to the first excited state (\tilde{A}) of 2-furanyloxy, and the features above 4.5 eV should represent the onset of the transition to the second excited state (\tilde{B}), as shown more clearly in the inset of Figure 2. The 0–0 transition (a) of band \tilde{A} at 3.90 eV defines an excitation energy of 2.14 eV, whereas the onset of band \tilde{B} at 4.58 eV gives rise to an excitation energy of 2.82 eV. We computed the excitation energy of the \tilde{A} state to be 1.50 eV, as compared with the experimental data in Table S2. We could not compute the excitation energy of the \tilde{B} state because it has the same symmetry as the ground state. The corresponding valence molecular orbitals (MOs) for the first three detachment channels of 2-furanyloxide are shown in Figure S3. The HOMO and HOMO–2 are both π orbitals of a'' symmetry, whereas the HOMO–1 with a' symmetry represents an in-plane O 2p lone pair with a weak antibonding π interaction with the carbon atom on the furanic ring. The distinct $s + d$ PE angular distributions for all three detachment channels are consistent with the nature of the MOs, as also indicated by their anisotropy parameters (Table S2).

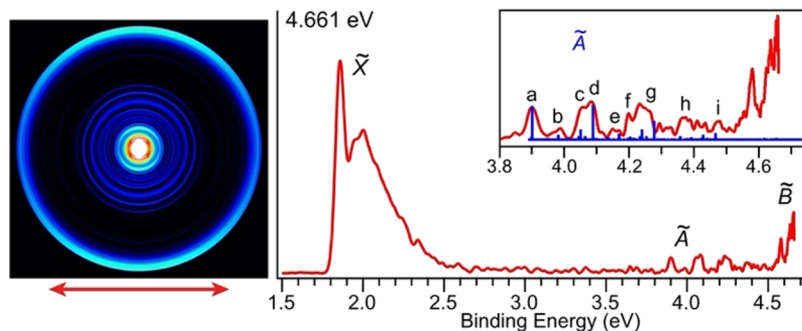


Figure 2. Photoelectron image and spectrum of 2-furanyloxide at 4.661 eV. In addition to the ground state (\tilde{X}), transitions to two excited states of 2-furanyloxy, \tilde{A} and \tilde{B} , are observed. The inset shows the comparison between the vibrational features (labeled as *a* to *i*) of the \tilde{A} state and the calculated FC factors. The double arrow below the image indicates the laser polarization direction.

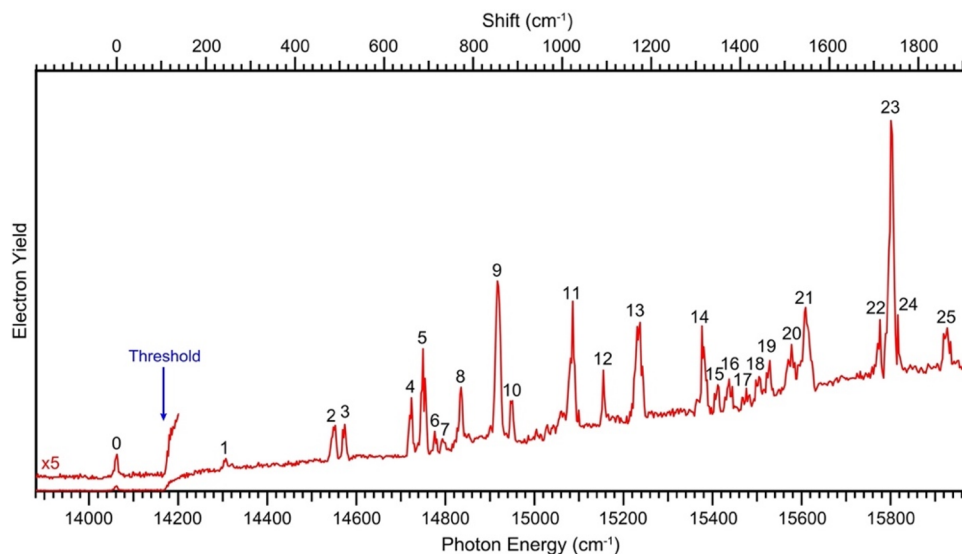


Figure 3. Photodetachment spectrum of cryogenically cooled 2-furanyloxide anion. The top axis indicates the shifts relative to peak 0.

Nine vibronic peaks are resolved for the \tilde{A} state, and they are labeled with lower case letters *a* to *i* (see the inset of Figure 2). Using the optimized structure of the first excited state of 2-furanyloxy (Figure S1c), we also performed FC calculations for the transitions to the \tilde{A} state to further confirm the assignment using the computed frequencies scaled by a factor of 0.95 (Table S6). The FC simulation is compared with the experimental data in the inset of Figure 2 by aligning the 0–0 transition with peak *a*. The good agreement between the FC simulation and the experimental data allowed us to assign the vibronic features for the \tilde{A} state, as given in Table S3. Three FC-active modes, ${}^{\text{A}}\nu_4$, ${}^{\text{A}}\nu_7$, and ${}^{\text{A}}\nu_{14}$ (the superscript “A” is used to denote the modes of the first excited state), are observed for the \tilde{A} state, all with a' symmetry. The most FC-active mode is ${}^{\text{A}}\nu_4$, which is approximately the C–O stretching mode (Figure S7). It is interesting to note that the structure of the \tilde{A} state (Figure S1c) represents an alkoxy radical, with a large C–O bond length between the furanic C and the methoxy O atom. The structural change of the \tilde{A} state relative to the anion and its alkoxy nature are consistent with the detachment from the HOMO–1, an in-plane O 2p lone pair (Figure S3b).

The 2-furanyloxy radical was calculated to have a dipole moment of 4.13 D,¹⁹ suggesting that 2-furanyloxide should have a DBS as an electronically excited state below its detachment threshold.²⁷ To search for the DBS, we performed PDS by monitoring the total electron yield as a function of

wavelength across the detachment threshold, in the energy range from 13 880 cm^{-1} (1.7209 eV) to 15 970 cm^{-1} (1.9800 eV), as shown in Figure 3. Electron signals appeared promptly at the detachment threshold of 14 174 cm^{-1} (arrow in Figure 3), indicating an *s*-partial-wave for the outgoing electrons according to the Wigner threshold law,⁴⁸ consistent with the π -type HOMO of 2-furanyloxide (Figure S3a). The gradually increasing baseline above the threshold represents the nonresonant photodetachment cross section, while the sharp resonant peaks indicate the existence of a DBS, as a result of excitation to specific vibrational levels of the DBS, followed by vibrational autodetachment. The weak peak observed below the threshold (labeled as 0) corresponds to the bound zero-point level of the DBS, and the resonant peaks above the threshold are also known as vibrational Feshbach resonances. The binding energy of the DBS, defined as the energy separation between the detachment threshold and the zero-point level of the DBS, is measured to be $115 \pm 6 \text{ cm}^{-1}$ ($0.0143 \pm 0.0008 \text{ eV}$). A total of 25 Feshbach resonances (labeled as 1 to 25) are observed in the scanned energy range. The wavelengths and photon energies for all the observed DBS vibrational levels are given in Table S4, as well as their shifts relative to the 0–0 level, their assignments, and comparison with the computed frequencies of the 2-furanyloxy radical (Table S5). For some of the Feshbach resonances, such as resonant peaks 3, 5, 11, 13–20, and 25, rotational profiles can

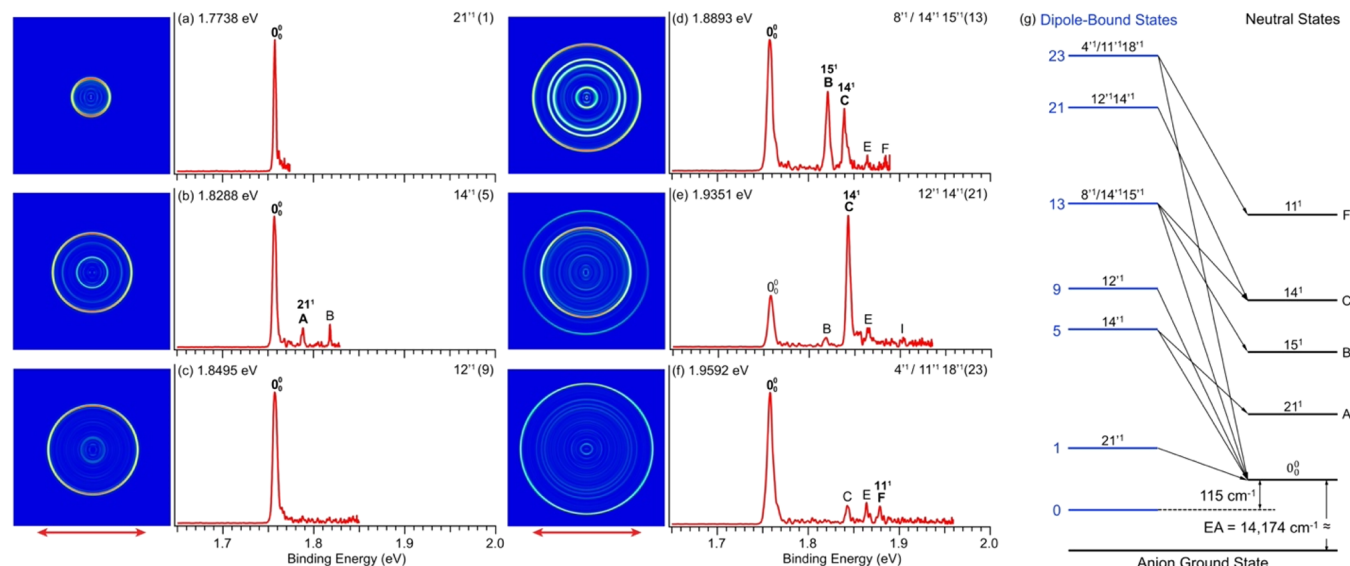


Figure 4. Selected resonant PE images and spectra of 2-furanyloxide at (a) $14\ 306\text{ cm}^{-1}$ (1.7738 eV), (b) $14\ 750\text{ cm}^{-1}$ (1.8288 eV), (c) $14\ 917\text{ cm}^{-1}$ (1.8495 eV), (d) $15\ 238\text{ cm}^{-1}$ (1.8893 eV), (e) $15\ 607\text{ cm}^{-1}$ (1.9351 eV), and (f) $15\ 802\text{ cm}^{-1}$ (1.9592 eV). The enhanced peaks are labeled in boldface. The wavelengths and assignments of the DBS vibrational levels are given, as well as the resonant peak numbers from Figure 3 in the parentheses. The double arrows below the images indicate the laser polarization. (g) Schematic energy level diagram for autodetachment from the vibrational levels of the DBS of 2-furanyloxide to the related neutral final states, corresponding to the six resonant PE spectra in Figure 4a–f, which correspond to peaks 1, 5, 9, 13, 21, and 23 in Figure 3.

be discerned. As we have shown previously,^{33,49,50} the rotational temperatures of anions in our cryogenic Paul trap were about 30–35 K.

By tuning the detachment laser to the Feshbach resonances of the DBS, we obtained 25 resonantly enhanced PE spectra, as shown in Figure 4, corresponding to resonant peaks 1, 5, 9, 13, 21, and 23. Additional resonant PE spectra are given in Figure S4 for resonant peaks 2–4, 6–8, 10–12, and 16 and Figure S5 for resonant peaks 14, 15, 17–20, 22, 24, and 25. Compared to the nonresonant PE spectra in Figure 1, the resonant PE spectra are highly non-Franck–Condon, where one or more vibrational peaks are enhanced (labeled in bold face in Figures 4, S4, and S5). In general, two detachment processes contribute to the rPES: (1) nonresonant photodetachment represented by the smooth baseline in the PDS (Figure 3) and (2) resonantly enhanced autodetachment via the vibrational levels of the DBS. The latter is governed by the $\Delta v = -1$ propensity rule, i.e., only one vibrational quantum can be coupled with the dipole-bound electron during autodetachment.^{51,52} This is because the highly diffuse dipole-bound electron has little effect on the structure of the neutral radical core, which means that the vibrational frequencies of the DBS are the same as those for the ground state of the 2-furanyloxy radical. Thus, the observed vibrational levels of the DBS can be assigned readily using the $\Delta v = -1$ propensity rule and the calculated vibrational frequencies for the 2-furanyloxy radical (Table S5).

Take resonant peak 1 as an example, where the resonant PE spectrum in Figure 4a was taken. The 0_0^0 transition is enhanced in the resonant PE spectrum, indicating autodetachment from a fundamental vibrational level of the DBS. The excitation energy for resonant peak 1 is measured to be 247 cm^{-1} (Table S4), relative to the zero-point level of the DBS, which agrees well with the calculated frequency for the ν_{21} mode (252 cm^{-1} , Table S5), the lowest frequency bending mode of the 2-furanyloxy radical (Figure S6). Thus, the weak

resonant peak 1 can be assigned confidently to $21'$ (the prime ' indicates the DBS vibrational mode). In addition to Figure 4a, PE spectra taken at resonant peaks 2–12 all display enhanced 0_0^0 transitions (Figures 4 and S4), indicating they are all due to autodetachment from fundamental excitations of different vibrational modes of the DBS. The respective DBS vibrational levels are given in the resonant PE spectra (Figures 4 and S4) and also in Table S4. Resonant peaks 1 ($21'$), 3 ($20'$), 4 ($19'$), 6 ($18'$), 8 ($17'$), and 10 ($16'$) are all due to excitation to bending modes with a'' symmetry (Figure S6), which are symmetry-forbidden and are usually not observed in nonresonant PE spectra. The observation of all six bending modes for the DBS of 2-furanyloxide is again a manifestation of the power of PDS to obtain vibrational information about polar radical species.

A number of resonant PE spectra taken at peaks 13, 15–19, 21, 22, 24, and 25 (Figures 4, S4, and S5) reveal an enhanced peak C ($14'$), which corresponds to the fundamental excitation of the highly FC-active mode ν_{14} with a measured vibrational frequency of 693 cm^{-1} (Table S1 and Figure S6). Thus, many of the resonant peaks in the PDS involve combinational vibrational levels of ν_{14}' . For example, Figure 4e taken at resonant peak 21 is due to excitation to the $12'14'1$ combinational level of the DBS. Coupling of one quantum of the ν_{12}' mode with the dipole-bound electron results in the enhancement of peak C ($14'$). In principle, coupling of one quantum of the ν_{14}' mode should result in an enhanced peak E ($12'$), which was not observed due to the much stronger coupling of the ν_{12}' mode with the dipole-bound electron. Such mode-specific vibronic coupling was first observed in the DBS of cryogenically cooled phenoxide anions.³⁴ In fact, such mode-specific vibronic coupling involving the ν_{14}' mode was also observed in Figures S5b–e,g,h. Recently, the autodetachment lifetimes of the different vibrational Feshbach resonances of phenoxide have been studied using the time-resolved experiment.⁵³ The resonant peak 13 contained excitation to

Table 1. Observed DBS Vibrational Peaks for the 2-Furanyloxide Spectra Shown in Figure 4a–f, Their Wavelengths, Energies in cm^{-1} , Shifts Relative to the DBS Zero-Point Level (peak 0), Assignments, and Comparison with the Computed Frequencies^a

Peak	Photon energy (cm^{-1}) ^b	Shift relative to peak 0 (cm^{-1})	Assignment	Theoretical frequency (cm^{-1}) ^c	Corresponding PES vibrational peaks
0	14 059(5)	0	zero-point level		
1	14 306(5)	247	21' ¹	252	A
5	14 750(5)	691	14' ¹	684	C
9	14 917(5)	858	12' ¹	872	E
13	15 238(5)	1179	8' ¹ /14' ¹ 15' ¹	1200/	I
21	15 607(5)	1548	12' ¹ 14' ¹		L
23	15 802(5)	1743	4' ¹ /11' ¹ 18' ¹	1764/	M

^aThe corresponding PES peaks in the non-resonant PE spectrum are also given. ^bThe numbers in the parentheses indicate the experimental uncertainties in the last digit. ^cThe vibrational frequencies are calculated at the B3LYP/6-311++G(d,p) level of theory.

two overlapping vibrational levels of 8'¹/14'¹15'¹, as shown in Figure 4d. The 8'¹ resonance resulted in the enhancement of the 0₀⁰ transition, while the 14'¹15'¹ combinational level led to the enhancement of the 15¹ (B) and 14¹ (C) final states. The resonant PE spectra presented in Figures 4f and S5c,e,f,i all involve overlapping combinational vibrational levels, resulting in multiple enhanced final states.

Because the ν_{14}' mode is one of the most FC-active modes, excitation to its overtone, resonant peak 16 (14'²), was also observed, resulting in the enhancement of the 14¹ (C) final state in the resonant PE spectrum (Figure S4j) according to the $\Delta v = -1$ propensity rule. Similarly, the vibrational overtone for mode ν_{19}' (19'²) is also observed to be overlapped with 7'¹ (peak 14 in Figure 3), resulting in the strong enhancement of peak α (19¹) in Figure S5a, in addition to the enhancement of the 0₀⁰ transition. The mode ν_{19} is an out-of-plane bending mode with a'' symmetry (Figure S6), and the 19¹ final state is only observed in the resonant PE spectrum. The binding energy for peak α is measured to be 659 cm^{-1} above the 0₀⁰ transition (Table S1), in agreement with the measured frequency for the ν_{19}' mode (19'¹) of the DBS in the PD spectrum (peak 4 in Table 4). Several weak peaks, i.e., A in Figure 4b, B in Figure S4h, and D in Figure S4i, appeared to be enhanced, but they do not seem to obey the $\Delta v = -1$ propensity rule. Such weak nonmode-specific autodetachment has been observed in rPES previously and was attributed to inelastic scattering of the outgoing autodetached electron.⁵⁴

The assignments of the six Feshbach resonances that give rise to the six resonant PE spectra in Figure 4 are given in Table 1, whereas the autodetachment processes are schematically shown in Figure 4g. All the observed Feshbach resonances in the PD spectrum of Figure 3 are summarized in Table S4, and the corresponding autodetachment processes are schematically shown in Figure S8. We obtained the fundamental frequencies for 18 out of a total of 21 vibrational modes for the 2-furanyloxy radical in its ground state ($\tilde{\chi}$) and three vibrational modes for its first excited state (\tilde{A}), as summarized in Table 2. Only the three high-frequency modes involving C–H stretching were not observed for the ground electronic state of the 2-furanyloxy radical. Specifically, the vibrational frequencies for all six low-frequency bending modes (Table 2 and Figure S6) are obtained. No other spectroscopic experiments can yield such rich vibrational information. It should be pointed out that vibrational frequencies were measured previously for several modes of 2-furanyloxy in an Ar matrix,¹⁸ and they are given in Table 2 for comparison. All matrix data agree well with the current results; only the

Table 2. Measured Vibrational Frequencies for the 2-Furanyloxy Radical from the Current Study

vibrational mode	symmetry	experimental frequency (cm^{-1}) ^d	theoretical frequency (cm^{-1}) ^b	Ar matrix frequency (cm^{-1}) ^c
ν_{21}	a''	247(4)	252	
ν_{20}	a''	514(5)	521	
ν_{19}	a''	664(5)	674	
ν_{18}	a''	718(5)	728	714.3
ν_{17}	a''	775(2)	785	773.0
ν_{16}	a''	888(5)	891	
ν_{15}	a'	490(2)	490	
ν_{14}	a'	691(2)	684	
ν_{13}	a'	747(5)	737	
ν_{12}	a'	858(3)	872	
ν_{11}	a'	1026(5)	1046	
ν_{10}	a'	1077(9)	1072	
ν_9	a'	1094(5)	1109	
ν_8	a'	1179(4)	1200	1167.6
ν_7	a'	1317(2)	1345	1314
ν_6	a'	1409(10)	1419	
ν_5	a'	1462(5)	1489	1462.2
ν_4	a'	1743(3)	1764	1732.8
$^A\nu_{14}$	a'	632(93)	648 ^d	
$^A\nu_7$	a'	1264(83)	1214 ^d	
$^A\nu_4$	a'	1474(83)	1521 ^d	

^aBoth PES (Tables S1 and S3) and PDS (Table S4) are taken into consideration for determining the vibrational frequencies. The numbers in the parentheses indicate the experimental uncertainties in the last digit. ^bTheoretical values at the B3LYP/6-311++G(d,p) level of theory (Table S5). ^cFrom ref 18. ^dThe theoretical frequencies for the \tilde{A} excited state are scaled by a factor of 0.95 (see Table S6).

frequencies of the ν_4 and ν_8 modes seemed to exhibit a large matrix shift.

By tuning the detachment laser to the zero-point level of the DBS (peak 0 in Figure 3), we obtained the one-color resonant two-photon detachment (R2PD) PE image and spectrum at 14 059 cm^{-1} (1.7431 eV), as shown in Figure 5. A single peak at the low binding energy side is observed, as a result of detachment from the zero-point level of the DBS by the second photon. A distinct *p*-wave is observed in the photoelectron angular distribution, as expected from the *s*-like orbital of the DBS prepared by the absorption of the first photon. The asymmetry parameter (β) of the PE image is obtained to be 1.5, compared to 2 for an atomic *s* orbital.⁵⁵ The binding energy of the DBS could be roughly estimated from the R2PD PE spectrum to be $113 \pm 65 \text{ cm}^{-1}$ (0.014 ±

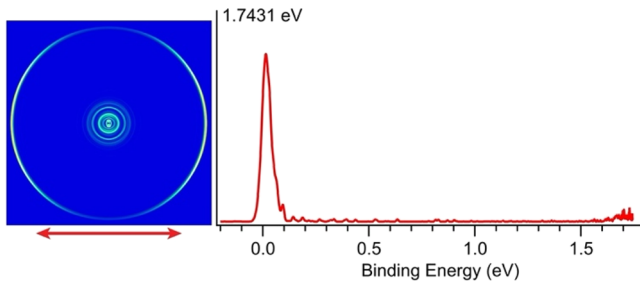


Figure 5. R2PD PE image and spectrum of 2-furanyloxide at the detachment wavelength of $14\ 059\ \text{cm}^{-1}$ (1.7431 eV), corresponding to the zero-point level of the DBS (peak 0 in Figure 3). The double arrow below the image indicates the polarization of the detachment laser.

$0.008\ \text{eV}$), compared to the accurate value of $115 \pm 6\ \text{cm}^{-1}$ obtained from the PD spectrum in Figure 3. It should be noted that there are no R2PD features in the high binding energy side in Figure 5, indicating there is no relaxation from the DBS zero-point level after the first photon absorption within the 5 ns detachment laser pulse, i.e., a long-lived DBS ($>5\ \text{ns}$). We have observed fast relaxations from the DBS of many anions previously,^{38,56,57} manifested as strong high binding energy features in the one-color R2PD PE spectra.

In conclusion, we report a combined high-resolution photoelectron spectroscopy, photodetachment spectroscopy, and resonant photoelectron imaging study of cryogenically cooled 2-furanyloxide anion ($\text{C}_4\text{H}_3\text{O}_2^-$). The photodetachment spectrum revealed a dipole-bound state $115 \pm 6\ \text{cm}^{-1}$ below the detachment threshold and 25 vibrational Feshbach resonances. By tuning the detachment laser to these resonances, we obtained 25 resonantly enhanced photoelectron spectra, which provided rich spectroscopic information for the 2-furanyloxy radical and aided the assignments of the vibrational levels of the dipole-bound state. The one-color resonant two-photon detachment image probes the nature of the dipole-bound state, revealing a dominantly *p*-wave angular distribution and a relatively long lifetime for the zero-point level of the dipole-bound state. The electron affinity of the 2-furanyloxy radical was measured accurately to be $14\ 174 \pm 6\ \text{cm}^{-1}$ ($1.7573 \pm 0.0008\ \text{eV}$). Frequencies for 18 vibrational modes were obtained for the ground electronic state of the 2-furanyloxy radical including all six bending modes, demonstrating the capability of the combination of photodetachment spectroscopy and resonant photoelectron spectroscopy for obtaining vibrational information for polar radical species via dipole-bound states. We also observed two electronic excited states of 2-furanyloxy at excitation energies of 2.14 and 2.82 eV above the ground state. The current study provides important vibrational and electronic information about the 2-furanyloxy radical, which should be valuable in understanding its reactivity and helping its detection in combustion processes.

ASSOCIATED CONTENT

Supporting Information

The Supporting Information is available free of charge at <https://pubs.acs.org/doi/10.1021/acs.jpcllett.2c03382>.

Experimental and theoretical details; optimized structures of the 2-furanyloxide anion and the 2-furanyloxy radical and its first electronic excited state; a comparison between the $21\ 119\ \text{cm}^{-1}$ (2.6185 eV) photoelectron spectrum and the computed Franck–Condon factors;

the anion valence molecular orbitals; additional resonant photoelectron spectra; the vibrational normal modes and their computed frequencies for the 2-furanyloxy radical and its first excited electronic state; a full schematic energy level diagram for the autodetachment processes of all the observed Feshbach resonances; tables of all the observed vibrational peaks in the photoelectron spectra and their assignments, the binding energies of the ground and excited states of 2-furanyloxy and comparison with theoretical calculations, the observed vibrational peaks of the first excited state of 2-furanyloxy and their assignments, the observed resonances in the photodetachment spectrum and their assignments, and the computed vibrational frequencies for the ground and first excited states of the 2-furanyloxy radical (PDF)

AUTHOR INFORMATION

Corresponding Authors

Dao-Fu Yuan – Department of Chemistry, Brown University, Providence, Rhode Island 02912, United States;
 • orcid.org/0000-0001-8461-6889; Email: daofu_yuan@brown.edu

Lai-Sheng Wang – Department of Chemistry, Brown University, Providence, Rhode Island 02912, United States;
 • orcid.org/0000-0003-1816-5738; Email: lai-sheng_wang@brown.edu

Author

Yue-Rou Zhang – Department of Chemistry, Brown University, Providence, Rhode Island 02912, United States

Complete contact information is available at:
<https://pubs.acs.org/10.1021/acs.jpcllett.2c03382>

Notes

The authors declare no competing financial interest.

ACKNOWLEDGMENTS

This work was supported by the Department of Energy, Office of Basic Energy Sciences, Chemical Sciences, Geosciences, and Biosciences Division under Grant DE-SC0018679 (to L.S.W.). The calculations were performed using resources from the Center for Computation and Visualization (CCV) of Brown University.

REFERENCES

- Ragauskas, A. J.; Williams, C. K.; Davison, B. H.; Britovsek, G.; Cairney, J.; Eckert, C. A.; Frederick, W. J., Jr.; Hallett, J. P.; Leak, D. J.; Liotta, C. L.; Mielenz, J. R.; Murphy, R.; Templer, R.; Tschaplinski, T. The Path Forward for Biofuels and Biomaterials. *Science* **2006**, *311*, 484–489.
- Havlík, P.; Schneider, U. A.; Schmid, E.; Böttcher, H.; Fritz, S.; Skálský, R.; Aoki, K.; Cara, S. D.; Kindermann, G.; Kraxner, F.; Leduc, S.; McCallum, I.; Mosnier, A.; Sauer, T.; Obersteiner, M. Global Land Use Implications of First and Second Generation Biofuel Targets. *Energy Policy* **2011**, *39*, 5690–5702.
- Beller, H. R.; Lee, T. S.; Katz, L. Natural Products as Biofuels and Bio-Based Chemicals: Fatty Acids and Isoprenoids. *Nat. Prod. Rep.* **2015**, *32*, 1508–26.
- Binder, J. B.; Raines, R. T. Simple Chemical Transformation of Lignocellulosic Biomass into Furans for Fuels and Chemicals. *J. Am. Chem. Soc.* **2009**, *131*, 1979–1985.
- Lange, J.-P.; van der Heide, E.; van Buijtenen, J.; Price, R. Furfural - A Promising Platform for Lignocellulosic Biofuels. *ChemSusChem* **2012**, *5*, 150–166.

- (6) Haro, P.; Ollero, P.; Villanueva Perales, Á. L.; Vidal-Barrero, F. Potential Routes for Thermochemical Biorefineries. *Biofuels, Bioprod. Bioref.* **2013**, *7*, 551–572.
- (7) Kubota, S. R.; Choi, K.-S. Electrochemical Valorization of Furfural to Maleic Acid. *ACS Sustainable Chem. Eng.* **2018**, *6*, 9596–9600.
- (8) Bruinsma, O. S. L.; Tromp, P. J. J.; de Sauvage Nolting, H. J. J.; Moulijn, J. A. Gas Phase Pyrolysis of Coal-related Aromatic Compounds in a Coiled Tube Flow Reactor. *Fuel* **1988**, *67*, 334–340.
- (9) Barckholtz, C.; Fadden, M. J.; Hadad, C. M. Computational Study of the Mechanisms for the Reaction of $O_2(^3\Sigma_g)$ with Aromatic Radicals. *J. Phys. Chem. A* **1999**, *103*, 8108–8117.
- (10) Fadden, M. J.; Hadad, C. M. Rearrangement Pathways of Arylperoxy Radicals. 2. Five-Membered Heterocycles. *J. Phys. Chem. A* **2000**, *104*, 6324–6331.
- (11) Tokmakov, I. V.; Kim, G.-S.; Kislov, V. V.; Mebel, A. M.; Lin, M. C. The Reaction of Phenyl Radical with Molecular Oxygen: A G2M Study of the Potential Energy Surface. *J. Phys. Chem. A* **2005**, *109*, 6114–6127.
- (12) Huber, G. W.; Iborra, S.; Corma, A. Synthesis of Transportation Fuels from Biomass: Chemistry, Catalysts, and Engineering. *Chem. Rev.* **2006**, *106*, 4044–4093.
- (13) Van Putten, R.-J.; van der Waal, J. C.; de Jong, E.; Rasrendra, C. B.; Heeres, H. J.; de Vries, J. G. Hydroxymethylfurfural, A Versatile Platform Chemical Made from Renewable Resources. *Chem. Rev.* **2013**, *113*, 1499–1597.
- (14) Hudzik, J. M.; Bozzelli, J. W. Structure and Thermochemical Properties of 2-Methoxyfuran, 3-Methoxyfuran, and Their Carbon-Centered Radicals Using Computational Chemistry. *J. Phys. Chem. A* **2010**, *114*, 7984–7995.
- (15) Simmie, J. M.; Somers, K. P.; Yasunaga, K.; Curran, H. J. A Quantum Chemical Study of the Abnormal Reactivity of 2-Methoxyfuran. *Int. J. Chem. Kinet.* **2013**, *45*, 531–541.
- (16) Hudzik, J. M.; Bozzelli, J. W. Thermochemistry of Hydroxyl and Hydroperoxide Substituted Furan, Methylfuran, and Methoxyfuran. *J. Phys. Chem. A* **2017**, *121*, 4523–4544.
- (17) Yamamoto, Y.; Ohno, M.; Eguchi, S. Study of 5-*Endo* Cyclization of 5-Oxapenta-2,4-Dienoyl Radical and Related Radicals by *Ab Initio* Calculation. Unusual Nonradical Cyclization Mechanism. *J. Org. Chem.* **1996**, *61*, 9264–9271.
- (18) Urness, K. N.; Guan, Q.; Troy, T. P.; Ahmed, M.; Daily, J. W.; Ellison, B.; Simmie, J. M. Pyrolysis Pathways of the Furanic Ether 2-Methoxyfuran. *J. Phys. Chem. A* **2015**, *119*, 9962–9977.
- (19) Abeysekera, C.; Hernandez-Castillo, A. O.; Stanton, J. F.; Zwier, T. S. Broadband Microwave Spectroscopy of 2-Furanyloxy Radical: Primary Pyrolysis Product of the Second-Generation Biofuel 2-Methoxyfuran. *J. Phys. Chem. A* **2018**, *122*, 6879–6885.
- (20) Weichman, M. L.; Neumark, D. M. Slow Electron Velocity-Map Imaging of Cryogenically Cooled Anions. *Annu. Rev. Phys. Chem.* **2018**, *69*, 101–124.
- (21) Zhu, G. Z.; Wang, L. S. High-resolution Photoelectron Imaging and Resonant Photoelectron Spectroscopy via Noncovalently Bound Excited States of Cryogenically Cooled Anions. *Chem. Sci.* **2019**, *10*, 9409–9423.
- (22) Desfrancois, C.; Abdoul-Carime, H.; Schermann, J. P. Ground-State Dipole-Bound Anions. *Int. J. Mod. Phys. B* **1996**, *10*, 1339–1395.
- (23) Compton, R. N.; Hammer, N. I. Multiple-Bound Molecular Anions. *Adv. Gas-Phase Ion Chem.* **2001**, *4*, 257–305.
- (24) Jordan, K. D.; Wang, F. Theory of Dipole -Bound Anions. *Annu. Rev. Phys. Chem.* **2003**, *54*, 367–396.
- (25) Hammer, N. I.; Hinde, R. J.; Compton, R. N.; Diri, K.; Jordan, K. D.; Radisic, D.; Stokes, S. T.; Bowen, K. H. Dipole-Bound Anions of Highly Polar Molecules: Ethylene Carbonate and Vinylene Carbonate. *J. Chem. Phys.* **2004**, *120*, 685–690.
- (26) Simons, J. Molecular Anions. *J. Phys. Chem. A* **2008**, *112*, 6401–6511.
- (27) Qian, C. H.; Zhu, G. Z.; Wang, L. S. Probing the Critical Dipole Moment to Support Excited Dipole-Bound States in Valence-Bound Anions. *J. Phys. Chem. Lett.* **2019**, *10*, 6472–6477.
- (28) Lykke, K. R.; Mead, R. D.; Lineberger, W. C. Observation of Dipole-Bound States of Negative Ions. *Phys. Rev. Lett.* **1984**, *52*, 2221–2224.
- (29) Mead, R. D.; Lykke, K. R.; Lineberger, W. C.; Marks, J.; Brauman, J. I. Spectroscopy and Dynamics of the Dipole-Bound State of Acetaldehyde Enolate. *J. Chem. Phys.* **1984**, *81*, 4883–4892.
- (30) Yokoyama, K.; Leach, G. W.; Kim, J. B.; Lineberger, W. C.; Boldyrev, A. I.; Gutowski, M. Autodetachment Spectroscopy and Dynamics of vibrationally excited Dipole-Bound States of H_2CCC^- . *J. Chem. Phys.* **1996**, *105*, 10706–10718.
- (31) Dessent, C. E. H.; Kim, J.; Johnson, M. A. Photochemistry of Halide Ion–Molecule Clusters: Dipole-Bound Excited States and the Case for Asymmetric Solvation. *Acc. Chem. Res.* **1998**, *31*, 527–534.
- (32) Mascalitolo, K. J.; Gardner, A. M.; Heaven, M. C. Autodetachment Spectroscopy of the Aluminum Oxide Anion Dipole Bound State. *J. Chem. Phys.* **2015**, *143*, 114311.
- (33) Liu, H. T.; Ning, C. G.; Huang, D. L.; Wang, L. S. Vibrational Spectroscopy of the Dehydrogenated Uracil Radical by Autodetachment of Dipole-Bound Excited States of Cold Anions. *Angew. Chem., Int. Ed.* **2014**, *53*, 2464–2468.
- (34) Liu, H. T.; Ning, C. G.; Huang, D. L.; Dau, P. D.; Wang, L. S. Observation of Mode-Specific Vibrational Autodetachment from Dipole-Bound State of Cold Anions. *Angew. Chem., Int. Ed.* **2013**, *52*, 8976–8979.
- (35) Huang, D. L.; Liu, H. T.; Ning, C. G.; Zhu, G. Z.; Wang, L. S. Probing the Vibrational Spectroscopy of the Deprotonated Thymine Radical by Photodetachment and State-Selective Autodetachment Photoelectron Spectroscopy via Dipole-Bound States. *Chem. Sci.* **2015**, *6*, 3129–3138.
- (36) Zhu, G. Z.; Huang, D. H.; Wang, L. S. Conformation-Selective Resonant Photoelectron Imaging from Dipole-Bound States of Cold 3-Hydroxyphenoxide. *J. Chem. Phys.* **2017**, *147*, 013910.
- (37) Zhu, G. Z.; Qian, C. H.; Wang, L. S. Dipole-Bound Excited States and Resonant Photoelectron Imaging of Phenoxide and Thiophenoxide Anions. *J. Chem. Phys.* **2018**, *149*, 164301.
- (38) Zhu, G. Z.; Cheung, L. F.; Liu, Y.; Qian, C. H.; Wang, L. S. Resonant Two-Photon Photoelectron Imaging and Intersystem Crossing from Excited Dipole-Bound States of Cold Anions. *J. Phys. Chem. Lett.* **2019**, *10*, 4339–4344.
- (39) Yuan, D. F.; Liu, Y.; Qian, C. H.; Zhang, Y. R.; Rubenstein, B. M.; Wang, L. S. Observation of a π -type Dipole-Bound State in Molecular Anions. *Phys. Rev. Lett.* **2020**, *125*, 073003.
- (40) Qian, C. H.; Zhang, Y. R.; Yuan, D. F.; Wang, L. S. Photodetachment Spectroscopy and Resonant Photoelectron Imaging of Cryogenically-Cooled 1-Pyrenolate. *J. Chem. Phys.* **2021**, *154*, 094308.
- (41) Zhang, Y. R.; Yuan, D. F.; Wang, L. S. Probing the Strong Nonadiabatic Interactions in the Triazolyl Radical using Photodetachment Spectroscopy and Resonant Photoelectron Imaging of Cryogenically Cooled Anion. *J. Am. Chem. Soc.* **2022**, *144*, 16620–16630.
- (42) Wang, L. S. Electrospray Photoelectron Spectroscopy: From Multiply-Charged Anions to Ultracold Anions. *J. Chem. Phys.* **2015**, *143*, 040901.
- (43) Wang, X. B.; Wang, L. S. Development of a Low-Temperature Photoelectron Spectroscopy Instrument Using an Electrospray Ion Source and a Cryogenically Controlled Ion Trap. *Rev. Sci. Instrum.* **2008**, *79*, 073108.
- (44) León, I.; Yang, Z.; Liu, H. T.; Wang, L. S. The Design and Construction of a High-Resolution Velocity-Map Imaging Apparatus for Photoelectron Spectroscopy Studies of Size-Selected Clusters. *Rev. Sci. Instrum.* **2014**, *85*, 083106.
- (45) Pugliesi, I.; Müller-Dethlefs, K. The Use of Multidimensional Franck-Condon Simulations to Assess Model Chemistries: A Case Study on Phenol. *J. Phys. Chem. A* **2006**, *110*, 4657–4667.
- (46) Zhang, Y. R.; Yuan, D. F.; Wang, L. S. Probing the Strong Nonadiabatic Interactions in the Triazolyl Radical using Photodetachment Spectroscopy and Resonant Photoelectron Imaging of

- Cryogenically Cooled Anion. *J. Am. Chem. Soc.* **2022**, *144*, 16620–16630.
- (47) Ichino, T.; Andrews, D. H.; Rathbone, G. J.; Misaizu, F.; Calvi, R. M. D.; Wren, S. W.; Kato, S.; Bierbaum, V. M.; Lineberger, W. C. Ion Chemistry of 1*H*-1,2,3-Triazole. *J. Phys. Chem. B* **2008**, *112*, 545–557.
- (48) Wigner, E. P. On the Behavior of Cross Sections Near Thresholds. *Phys. Rev.* **1948**, *73*, 1002–1009.
- (49) Huang, D. L.; Zhu, G. Z.; Wang, L. S. Observation of Dipole-Bound State and High-Resolution Photoelectron Imaging of Cold Acetate Anions. *J. Chem. Phys.* **2015**, *142*, 091103.
- (50) Zhu, G. Z.; Liu, Y.; Wang, L. S. Observation of Excited Quadrupole-Bound States in Cold Anions. *Phys. Rev. Lett.* **2017**, *119*, 023002.
- (51) Berry, R. S. Ionization of Molecules at Low Energies. *J. Chem. Phys.* **1966**, *45*, 1228–1245.
- (52) Simons, J. Propensity Rules for Vibration-Induced Electron Detachment of Anions. *J. Am. Chem. Soc.* **1981**, *103*, 3971–3976.
- (53) Kang, D. H.; An, S.; Kim, S. K. Real-Time Autodetachment Dynamics of Vibrational Feshbach Resonances in a Dipole-Bound State. *Phys. Rev. Lett.* **2020**, *125*, 093001.
- (54) Huang, D. L.; Liu, H. T.; Ning, C. G.; Dau, P. D.; Wang, L. S. Resonant Photoelectron Imaging of Deprotonated Uracil Anion via Vibrational Levels of a Dipole-Bound Excited State. *Chem. Phys.* **2017**, *482*, 374–383.
- (55) Cooper, J.; Zare, R. N. Angular Distribution of Photoelectrons. *J. Chem. Phys.* **1968**, *48*, 942–943.
- (56) Zhang, Y. R.; Yuan, D. F.; Qian, C. H.; Wang, L. S. Observation of a Dipole-Bound Excited State in 4-Ethynylphenoxide and Comparison with the Quadrupole-Bound Excited State in the Isoelectronic 4-Cyanophenoxide. *J. Chem. Phys.* **2021**, *155*, 124305.
- (57) Yuan, D. F.; Zhang, Y. R.; Qian, C. H.; Wang, L. S. Resonant Two-Photon Photoelectron Imaging and Adiabatic Detachment Processes from Bound Vibrational Levels of Dipole-Bound States. *Phys. Chem. Chem. Phys.* **2022**, *24*, 1380–1389.

□ Recommended by ACS

Dipole-Bound State, Photodetachment Spectroscopy, and Resonant Photoelectron Imaging of Cryogenically-Cooled 2-Cyanopyrrolide

Dao-Fu Yuan, Lai-Sheng Wang, et al.

SEPTEMBER 12, 2022

THE JOURNAL OF PHYSICAL CHEMISTRY A

READ ▶

Rotational Cooling Effect on the Rate Constant in the CH₃F + Ca⁺ Reaction at Low Collision Energies

Kunihiro Okada, Hans A. Schuessler, et al.

JULY 20, 2022

THE JOURNAL OF PHYSICAL CHEMISTRY A

READ ▶

Ultracold Sticky Collisions: Theoretical and Experimental Status

Roman Bause, Xin-Yu Luo, et al.

JANUARY 09, 2023

THE JOURNAL OF PHYSICAL CHEMISTRY A

READ ▶

Infrared Spectroscopy of (Benzene-H₂S-X_n)⁺, X = H₂O (n = 1 and 2) and CH₃OH (n = 1), Radical Cation Clusters: Microsolvation Effects on the S-π Hemibond

Takeru Kato and Asuka Fujii

JANUARY 13, 2023

THE JOURNAL OF PHYSICAL CHEMISTRY A

READ ▶

Get More Suggestions >